Hindawi
Advances in Civil Engineering
Volume 2022, Article ID 6807916, 13 pages
https://doi.org/10.1155/2022/6807916

Research Article

Seismic Response Analysis of Multidimensional and Multiangle Long-Span Top-Supported CFST Arch Bridge

Zite Li,[1,2] **Genhui Wang**,[1] **Jiang Fan**,[2] **Weihong Wu**,[2] **Yue Jian**,[3] **and Xiaozhong Li**[1]

[1]*School of Civil Engineering, Lanzhou Jiaotong University, Lanzhou, Gansu 730070, China*
[2]*Gansu Province Transportation Planning, Survey & Design Institute Co Ltd, Lanzhou, Gansu 730030, China*
[3]*Department of Basic Sciences, Lanzhou Institute of Technology, Lanzhou, Gansu 730050, China*

Correspondence should be addressed to Genhui Wang; wahl@mail.lzjtu.cn

Received 18 June 2022; Revised 13 October 2022; Accepted 19 October 2022; Published 3 November 2022

Academic Editor: Wonseok Chung

Taking a concrete-filled steel tube (CFST) arch bridge with a clear span of 400 m as an example, the in-depth analysis of its natural vibration characteristics is carried out by establishing a finite element model. Then, the three-dimensional El Centro recorded wave after amplitude modulation is taken as the excitation wave; the structural response under three kinds of single dimension and four kinds of multidimensional combined excitation and 0~90° transformation X(longitudinal) + Y(transverse) orthogonal combined excitation is evaluated. The results show that the structure of long-span top-supported arch bridge extends in the longitudinal and vertical dimensions at the same time, and the mode shape density and mass distribution have multidirection and multiangle coupling. With the increase of excitation dimensions, the value and relative ratio of chord axial force increase. The maximum axial force ratio of $X + Y$ to X and Y is 2.1, the maximum axial force ratio of $X + Y + Z$ (longitudinal) to $X + Y$, $X + Z$, and $Y + Z$ is 1.4, 1.8, and 1.8; the displacement in X and Y direction under combined excitation is independent and the displacement in Z direction is its coupling term, but the displacement under $X + Y + Z$ combined excitation is only 10% larger than that under $X + Z$ and $Y + Z$ combined excitation. Under the combined excitation of $X + Y$ with a changing angle of 0°~90°, the axial force variation of the chord at different positions and on the same section of the arch rib has spatial characteristics. The variation range of upper and lower rod axial force varies from 0.63 to 1.35 and from 0.81 to 1.51, respectively, the change trend of displacement in the X and Y directions is relatively consistent, the change of displacement in the Z direction is asynchronous, and the displacement of vault section increases by one time. The seismic response of this bridge type under multidimensional and multiangle excitation shows obvious superposition.

1. Introduction

In the past 20 years, China's concrete-filled steel tubular arch bridges have experienced a relatively centralized breakthrough in terms of construction span, quality, and quantity, and the country still maintains a leading position globally in the construction of arch bridges [1]. However, in recent decades, large earthquakes in high-intensity earthquake zones have seriously threatened human security and caused large losses to the national economy. Bridges play an important role in postdisaster rescue and reconstruction activities, and seismic research has been paid increasing attention by scholars at home and abroad [2]. The mass distribution of the long-span deck concrete-filled steel tubular arch bridge is greater than that of the abutment exerted onto the ground, resulting in the dynamic characteristics of the structure, such as long natural vibration period, small vibration damping ratio, a significant influence of high-order vibration modes, and large differences in the natural vibration characteristics of various components [3].

Both the results of earthquake damage assessment and vibration theory research show that an earthquake can be decomposed into three orthogonal translation components and three orthogonal rotation components [4, 5]. Due to the differentiated focal mechanism, variable wave transmission medium [6], and the uncertainty of seismic wave transmission direction and angle [7], multiple orthogonal degrees of freedom of ground motion are often coupled. It is clearly

insufficient to study only one-dimensional seismic action, and the multidimensional coupling of ground motion also needs to be considered [8]. Xue et al. [9] summarized the input problem and calculation method of multidimensional ground motion of structures. Zhang et al. [10] studied the spatial response of long-span deck railway steel truss arch bridge under multidimensional seismic excitation. Farahmand-Tabar and Barghian [11] conducted three-component orthotropic seismic excitation analysis on the hybrid beam of a long-span concrete-filled steel tubular arch bridge and a cable-stayed bridge. Huang et al. [12] performed an experimental study on the seismic performance of a concrete-filled steel tubular arch bridge using multiple shaking table excitation. Luo et al. [13] studied the seismic response of arch bridges of various materials and structural forms by using the excitation mode of independent input and simultaneous input in three orthogonal directions. Chen and Guo [14] examined the structural response of a half-through continuous steel truss tied arch bridge under one-way and two-way ground motion inputs. Dai et al. [15] analyzed the vibration control of the tower under multidimensional seismic excitation. Zhao and Zhou [16] investigated the structural response of a long-span concrete-filled steel tubular basket arch bridge under multidimensional seismic excitation. Zhang et al. [17] used the pseudoexcitation method to comprehensively analyze the structural response of a concrete-filled steel tubular arch bridge under three-dimensional space earthquake. Li et al. [18] analyzed the structural response of a long-span continuous beam arch bridge under multisupport and multidimensional earthquakes. The above results show that the structural response of a long-span arch bridge under multidimensional seismic excitation needs further study. At the same time, when the time history method is used to analyze the response of bridges under multidimensional seismic action, the seismic input angle is different, and the structural response also varies. Only when the seismic wave is input into a specific direction, a certain type of component on a certain section can reach the control value. To determine the most unfavorable seismic input angle of a certain structural response control value, many scholars have compared the seismic wave input results in different directions. Li et al. [19], Wang et al. [20], and Liu et al. [21] analyzed the seismic response of a cable-stayed bridge by changing the main seismic input direction. The results showed that the seismic motion direction has an impact on the dynamic characteristics and seismic response. Sun et al. [22] transformed the angle of the orthogonal recorded wave to synthesize the seismic wave in the main direction and analyzed the frame structure. The findings revealed that the dynamic response is greatly affected by the input angle of the seismic wave. Zhang et al. [23] estimated the incident angle of seismic waves by using vibration response data and a superposition integration algorithm and analyzed the seismic response of the dam under different input angles. Shen et al. [24] used OPENSEES to analyze the vulnerability of a high-speed railway circular pier under multidimensional earthquake, and the results showed that the seismic input angle has a significant impact on the dynamic response of the fixed middle pier along the bridge direction. The aforementioned studies demonstrated that the main direction of seismic wave input cannot be ignored. The above two types of research correspond to the response analysis of a single arch rib under multidimensional seismic excitation or multiangle seismic excitation. The section of long-span concrete-filled steel tubular truss arch bridge itself has certain spatial characteristics, and it is more practical to combine multidimensional and multiangle excitation to study the seismic response of upper and lower chords in the seismic design.

In this study, a 400-m deck concrete-filled steel tubular highway arch bridge in a high seismic region in Northwest China is taken as the research object, and the El Centro three-dimensional seismic wave, modified according to the effective peak acceleration and site type in the safety assessment report, is used as the time history excitation function. Then, the axial force and displacement response analysis under 7 kinds of combined excitation of single dimension and multidimension and X(longitudinal) + Y(transverse) orthogonal combined excitation of 0°~90° transformation angle are carried out.

2. Project Overview

The highway bridge of this study adopts the design standard of two-way, 4 lanes, and 80 km/h maximum speed, with the main bridge being a 400 m top-loaded concrete-filled steel tube (CFST) arch bridge. The bridge deck is made from a steel floor corrugated web-concrete bridge deck composite beam, and the main arch ring has a four-limb concrete-filled steel tube double-arch rib space truss structure with equal width and variable height. It is fabricated by a cantilever assembly process of cable-stayed buckle + cable suspension. The peak acceleration of the horizontal basic ground motion is 0.2 g, the characteristic period is 0.45 s, the site category is Class I, and the fortification intensity is VIII.

The arch axis adopts a catenary with an arch axis coefficient of 1.55, the net span $L_0 = 400$ m, and the net sag height $f_0 = 80$ m. The height of the center of the chord varies from 7.5 m at the top of the vault to 14 m at the foot of the arch. The transverse center distance of each truss chord group is 4 m, and the transverse center distance between the two groups of trusses is 18 m. Closed "X"-shaped transverse joints are set in the vertical column, and they have a continuous arrangement. The "N"-shaped parallel connection, the chord, and the inclined web of the hinge shaft are made from C60 self-compacting compensating shrinkage steel tube concrete, and the rest are empty steel tubes. The arch rib is made from Φ1300 mm rolled welded steel pipe, and the web rod is made from Φ914 mm and Φ711 mm finished seamless steel pipes. The chords are manufactured from Q390D steel, and the rest are made from Q355D steel. The main bridge structure layout is shown in Figure 1.

3. Dynamic Analysis Model and Natural Vibration Characteristics

3.1. Finite Element Model. MIDAS/CIVIL analysis software is used to establish a three-dimensional finite element model of the bridge member. The deck of the bridge adopts plate

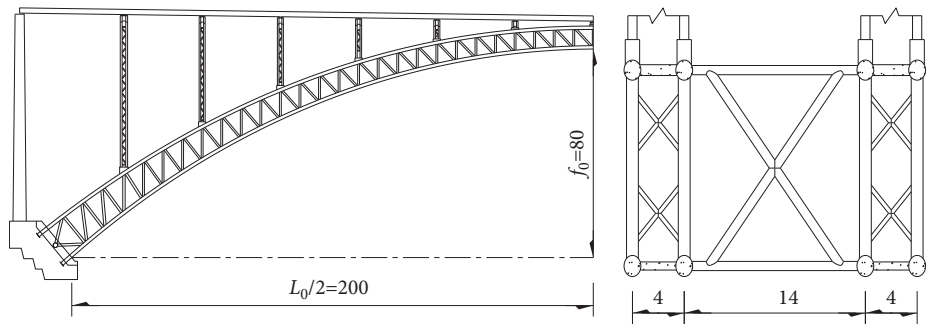

Figure 1: Main bridge structure layout (unit: m). (a) Half main bridge facade. (b) Typical cross-section of main arch ring.

elements, and the rest of the members have space beam elements. The elastic modulus of the CFST arch rib and vertical column section is calculated from the unified theory. The arch foot and the bottom of the junction pier have fixed restraints, columns 1~2 adopt a fixed bearing, and the other columns feature high damping rubber bearings. The finite element model of the full bridge is shown in Figure 2.

3.2. Solution of Multidimensional Seismic Dynamics Equation. The dynamic equation of the bridge under multidimensional earthquake action can be expressed as

$$[M]\{u\} + [C]\{\dot{u}\} + [K]\{u\} = -[M]\{u_g\}, \tag{1}$$

where $\{u\} = \{\{u\}_x^T, \{u\}_y^T, \{u\}_\theta^T\}$ represents the displacement motion of X, Y, and torsion directions relative to the ground, $\{u_g\} = \{u_{gx}, u_{gy}, 0\}^T$ is the ground motion acceleration vector, and $[M]$, $[C]$, $[K]$ is the 3N-dimensional mass matrix, damping matrix, and stiffness matrix of the structure, respectively [15]:

$$\{u\} = \sum_{n=1}^{3N} \{\phi_n\} q_n(t) = [\Phi]\{q\}, \tag{2}$$

where $\{q\} = \{q_1, q_2, \ldots, q_{3N}\}^T$ is a generalized coordinate vector and $[\Phi] = [\{\phi\}_1, \{\phi\}_2, \ldots, \{\phi\}_{3N}]$ is the mode matrix. By substituting equation (2) into equation (1), we can obtain

$$[M][\Phi]\{q\} + [C][\Phi]\{\dot{q}\} + [K][\Phi]\{q\} = -[M]\{u_g\}, \tag{3}$$

Formula (3) yields multiplication $\{\phi_2\}_n^T$. Using the orthogonal condition, we can obtain

$$q_n + 2\xi_n\omega_n\dot{q}_n + \omega_n^2 q_n = -\frac{\sum_{i=1}^{N} m_i\phi_n(i)u_{gx} + \sum_{i=N+1}^{2N} m_i\phi_n(i)u_{gy}}{\sum_{i=1}^{3N} m_i\phi_n^2(i)}, \tag{4}$$

which is abbreviated as

$$q_n + 2\xi_n\omega_n\dot{q}_n + \omega_n^2 q_n = -(\gamma_{xn}u_{gx} + \gamma_{yn}u_{gy}) \tag{5}$$

where $\gamma_{xn} = \sum_{i=1}^{N} m_i\phi_n(i)/\sum_{i=1}^{3N} m_i\phi_n^2(i)$ and $\gamma_{yn} = \sum_{i=N+1}^{2N} m_i\phi_n(i)/\sum_{i=1}^{3N} m_i\phi_n^2(i)$ represent the mode shape mass participation coefficient of the nth mode shape in the X and Y directions.

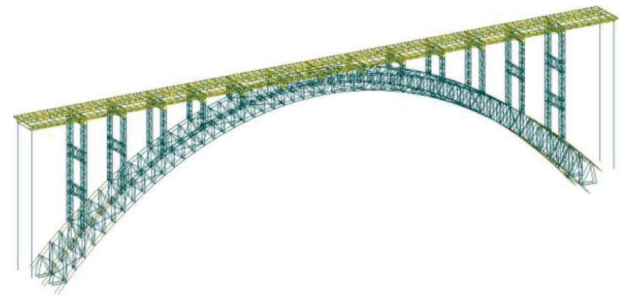

Figure 2: Full-bridge finite element model.

When the initial displacement and initial velocity of the structure are zero, the Duhamel integral is used to solve equation (5), which yields

$$\begin{aligned} q_n(t) &= -\frac{\gamma_n(x)}{\omega_{Dn}} \int_0^t u_{gx}(\tau) e^{-\xi_n\omega_n^{t-\tau}} \sin\omega_{Dn}(t-\tau)d\tau \\ &\quad -\frac{\gamma_n(y)}{\omega_{Dn}} \int_0^t u_{gy}(\tau) e^{-\xi_n\omega_n^{t-\tau}} \sin\omega_{Dn}(t-\tau)d\tau \\ &= \gamma_n(x)\delta_{nx}(t) + \gamma_n(y)\delta_{ny}(t). \end{aligned} \tag{6}$$

By substituting equation (6) into equation (2), the response under multidimensional earthquake action can be obtained.

3.3. Natural Vibration Characteristics. The natural vibration characteristics include the necessary parameters and important indicators for an in-depth analysis and judgment of the structural dynamic response and change trends [25]. Given that the damping ratio of the CFST structure is 0.03, the mode shape damping calculation method combining the mass and stiffness factors is selected, and the multiple Ritz vector method is used to solve the dynamic characteristics of the structure under the load condition of three-dimensional initial ground acceleration [26]. The density of mode shapes, the change of mode shape, and the participation coefficient of each mode shape in the direction of each degree of

freedom are established. The natural vibration frequency and mode shape description of the main arch are shown in Table 1, the mass distribution and mass participation coefficient of the first ten modes are listed in Figure 3, and the mode of the first mode is presented in Figure 4. *X*, *Y*, and *Z*, respectively, represent the longitudinal, transverse, and vertical direction of the bridge, *D* represents the translation along the coordinate axis, and *R* represents the rotation around the coordinate axis.

It can be seen from Table 1 and Figures 3 and 4 that the main mode shape of the arch rib is out-of-plane bending-torsional coupled vibration. The arch rib vibration modes include out-of-plane transverse bending and torsional vibrations around the longitudinal axis (DY-RX), planar torsional vibration around the vertical axis (RZ), in-plane vertical bending vibration (DZ), in-plane translational vibration along the bridge, and vertical bending coupled vibration (DX-RY). Vibration has multidirectional and multiangle coupling; that is, out-of-plane lateral vibration must be accompanied by torsional vibration around the longitudinal axis, and the torsional vibration around the horizontal axis must be accompanied by in-plane longitudinal translational vibration.

4. Seismic Input

The arch is placed in moderately weathered quartz diorite, which is a Class I hard soil site. According to the existing records of strong earthquakes, the El Centro recorded wave with similar site type, characteristic period, and spectral characteristics is selected as the excitation wave. According to the effective peak acceleration of the 50-year 2% exceedance probability (E2 level) in the earthquake safety assessment report, the amplitude modulation is corrected. The corrected values are shown in Table 2, and the corrected El Centro three-dimensional seismic waves are presented in Figure 5.

5. Multidimensional Seismic Excitation Response

Taking the corrected 3D El Centro recorded wave as the excitation wave, the time-history analysis method of linear elastic direct integration is used to analyze the *X*, *Y*, *Z*, $X+Y$, $X+Z$, $Y+Z$, and $X+Y+Z$ totals. The axial force and displacement responses of the upper and lower chord control sections of the arch rib under seismic excitation with seven-dimensional combinations are analyzed, and the response values under the multidimensional combined excitation and single-dimensional excitation are normalized. The CQC combination is used for multimode shape, and the SRSS combination is used for multidimensional input. The response values are all values after deducting the dead load effect after continuous time history analysis, that is, only the structural response values under earthquake action. The bridge is a truss arch rib structure with variable cross section. The change of the bending moment of single chord cannot fully reflect the change of bending response of the overall section of the main arch. The displacement response of the upper chord can be used to reflect the change of bending moment of the whole section. Under the action of earthquake, the arch rib produces alternating tension and pressure. The structural response value can be divided into two working conditions *N*max and *N*min for discussion, which is beneficial to the structural design of the corresponding envelope value.

5.1. Axial Force Response. It can be seen from Figure 6 and Tables 3 and 4 that the axial force of different sections under single direction excitation is different, the axial force of the same section under different direction excitation is different, and the axial force change of different sections under different direction excitation is random. The variation law of axial force under multidimensional excitation of top chord: the ratios of $X+Y$ to X and Y are 1.3~1.6 (vault 3.8) and 1.3~2.0 (vault 1.0), $X+Z$ to X and Z are 1.1~1.6 (vault 2.8) and 1.1~2.8 (arch foot 6.0), $Y+Z$ to Y and Z are 1.1~1.3 and 1.7~2.1 (arch foot 4.7), $X+Y+$Z to X, Y, and Z are 1.3~1.7 (vault 4.9), 1.3~1.9, and 1.9~3.1 (vault 6.9), and $X+Y+Z$ to $X+Y$, $X+Z$, and $Y+Z$ are 1.0~1.3, 1.1~1.8, and 1.0~1.5. The variation law of axial force under multidimensional excitation of bottom chord: the ratios of $X+Y$ to X and Y are 1.2~2.1 (vault 3.8) and 1.3~1.9 (vault 1.0), $X+Z$ to X and Z are 1.3~1.6 (vault 3.8) and 1.4~3.0 (vault 6.0), $Y+Z$ to Y and Z are 1.1~1.3 and 1.8~2.7, $X+Y+$Z to X, Y, and Z are 1.3~2.2 (vault 5.0), 1.4~2.1, and 1.9~3.5, and $X+Y+$Z to $X+Y$, $X+Z$, and $Y+Z$ are 1.0~1.4, 1.0~1.4, and 1.1~1.8. The structure is longitudinally symmetrical, the axial force of the vault under the *X* direction excitation is small, and the axial force ratio under the multidimensional excitation is large (the maximum is 5.0), but the *X* direction is not the single direction control excitation; the axial force ratio of multidimensional excitation to *Z* direction excitation is relatively large (the maximum is 6.9), but the axial force value of *Z* direction to *X* and *Y* direction excitation is smaller, *X* and *Y* are the main single direction excitation directions, and *Z* direction excitation has obvious superposition. With the increase of excitation dimension, the axial force value and relative ratio of each section are increasing, the maximum axial force ratio of $X+Y$ to X and Y is 2.1 (vault 3.8) and 2.0 (vault 1.0) and $X+Y+Z$ to $X+Y$, $X+Z$, and $Y+Z$ is 1.4, 1.8, and 1.8. Therefore, the axial force response of this type under multidimensional combined excitation is stackable.

5.2. Displacement Response. It can be seen from Figure 7 and Table 5 that the displacement ratio of multidimensional excitation to *X*-direction excitation is 1.0~1.2, the displacement ratio to *Y*-direction excitation is basically 1.0, and the displacement ratio of $X+Z$ excitation to *Z*-direction excitation is 3.7~4.5 (except for the vault). The displacement ratio of the $Y+Z$ excitation combination relative to *Z* direction excitation is 1.7~2.4, and the displacement ratio of $X+Y+Z$ excitation relative to *Z* direction excitation is 2.3~6.3. It shows that the displacement of *X* and *Y* directions under combined excitation is independent, and the displacement of *Z* direction is its coupling term, but the

Table 1: Main arch natural vibration characteristics.

Order	Frequency (Hz)	Mode shape description
1	0.24	Out-of-plane first-order bending and first-order torsional symmetric coupled vibration
2	0.32	Out-of-plane second-order antisymmetric torsional vibration
3	0.62	Out-of-plane third-order bending and third-order torsional symmetric coupled vibration
4	0.64	In-plane first-order antisymmetric bending vibration
5	0.80	Out-of-plane third-order bending and third-order torsional symmetric coupled vibration
6	0.82	Second-order symmetrical bending vibration in plane
7	0.88	Out-of-plane fourth-order torsional antisymmetric vibration
8	0.90	Out-of-plane second-order bending and first-order torsional symmetric coupled vibration
9	1.21	Out-of-plane third-order bending and third-order torsional symmetric coupled vibration
10	1.31	In-plane third-order antisymmetric bending vibration

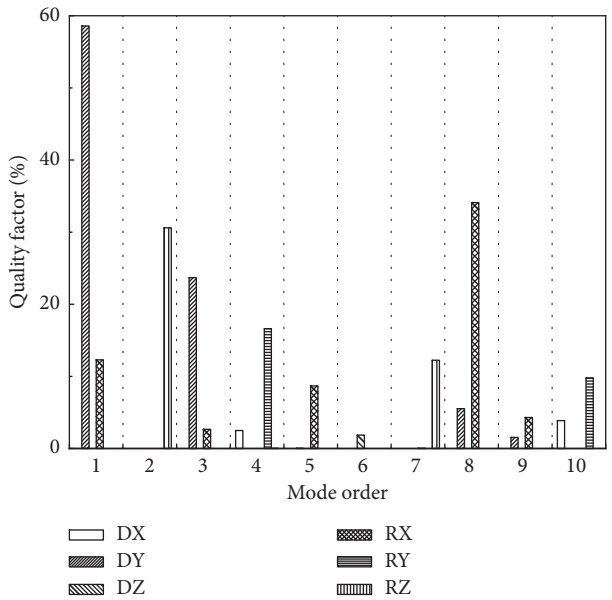

Figure 3: Mode shape mass participation coefficient.

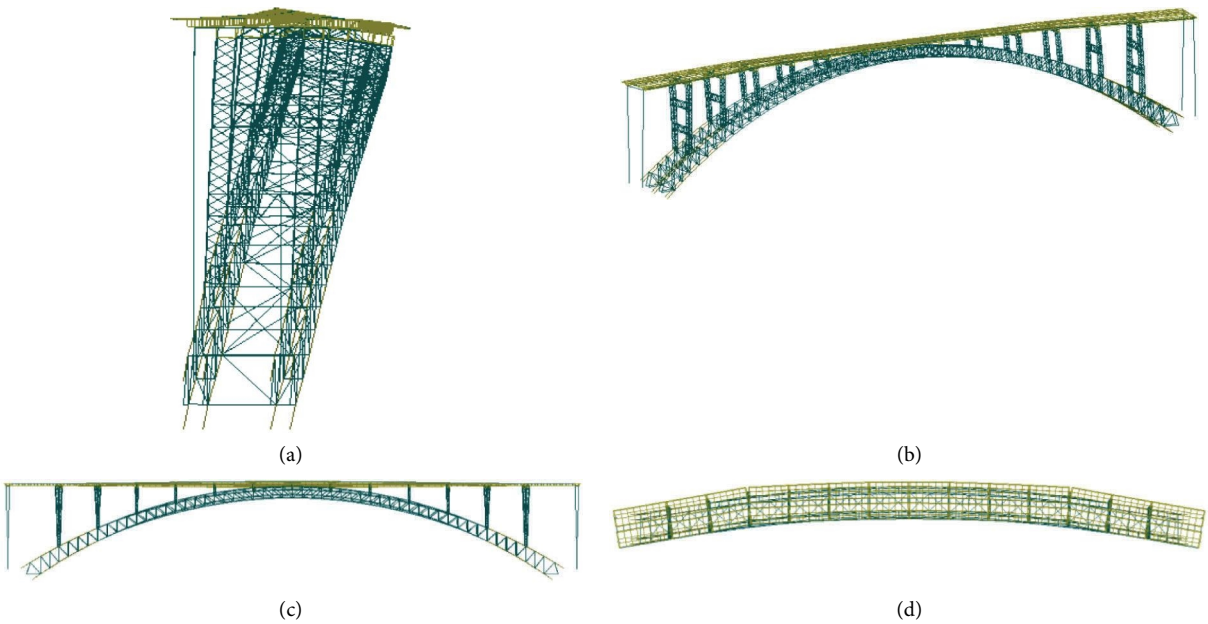

Figure 4: The first-order mode shape diagram of the main arch. (a) Side, (b) 3D, (c) facade, and (d) flat.

Table 2: Peak acceleration correction value (g).

Direction	Peak acceleration	Safety assessment effective peak acceleration	Fix coefficient	Corrected peak acceleration
NS(X)	0.21			0.24
EW(Y)	0.36	0.42	1.163	0.42
UD(Z)	0.25			0.29

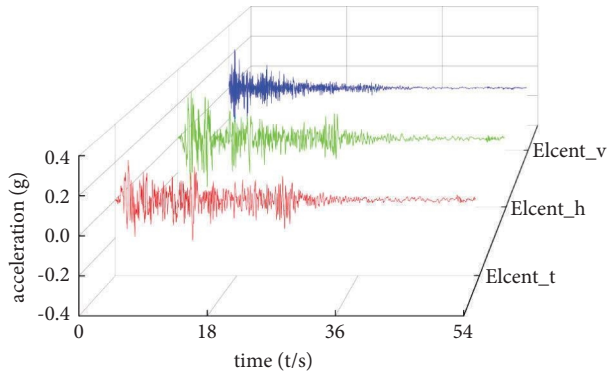

Figure 5: Corrected El Centro 3D seismic waves.

displacement of $X+Y+Z$ combined excitation is only 10% larger than that of $X+Z$ and $Y+Z$ combined excitation.

6. Multiangle Seismic Excitation Response

The records collected by strong earthquake stations are generally time histories along the three orthogonal directions of EW(X), NS(Y), and UD(Z). Therefore, a set of strong earthquake records with orthogonal horizontal directions can be transformed into Cartesian coordinates from 0° to 180° according to (Figure 8)

$$\begin{aligned} x'(t) &= x(t)\cos\theta + y(t)\sin\theta, \\ Y'(t) &= y(t)\cos\theta - x(t)\sin\theta. \end{aligned} \tag{7}$$

It can be seen from Figure 9 that when EW is used as the main axis direction transformation, it reaches a peak value of 0.404 g at 60° and 150°, and when NS is used as the main axis direction transformation, it reaches a peak value of 0.404 g at 30° and 120°. The acceleration in the cross direction is 0. At the same time, according to the change curve of the function of coordinate transformation formula (7), it can be seen that, with the difference of acceleration values in the two orthogonal directions of EW and NS in the original record, the angle of the maximum value after coordinate transformation is different, but the value is the same. Therefore, when the structure is relatively simple and the mode shape has obvious orthogonality, the seismic wave input in one direction can be transformed through the angle, and the time-history wave corresponding to the maximum acceleration peak value can be found as the control wave input. However, when the structure is relatively complex and the mode shapes have multidirectional coupling, as shown in the research results in the previous section, the structural response under multidimensional seismic excitation has a significant increase effect, and the $X+Y$ combined excitation can be used as the control combination input. Therefore, the orthogonal combination of transforming the EW and NS input angles at the same time should be used, and it is meaningful to study the seismic response of multiangle input. In view of the symmetry of the structure in the longitudinal bridge direction, the input angle of the $X+Y$ orthogonal combination can be transformed simultaneously from 0° to 90° for further research.

6.1. Axial Force Response. It can be seen from Figures 10 and 11 that, from the arch foot to the 1L/8 section, the axial force first decreases and then increases with the change of angle, and an inflection point appears near 20°. The maximum arch foot and 1L/8 section ratios are 1.35 and 1.28, respectively. The axial force of the lower chord varies, the arch foot axial force ratio at 80° is the largest at 1.32, and the 1L/8 section axial force ratio is the largest at 90° at 1.51. Near the 1L/4 section, the overall trend is declining, the upper and lower chords change synchronously, the minimum axial force ratio is 0.73/0.86, and the appearance time is 55° and 90°. Near the 3L/8 section, the upper chord axial force ratio of the rod shows a downward trend, with a minimum value of 0.87 near 70°, and then, the change tends to be gentle; the axial force ratio of the lower chord increases first and then decreases, but both are greater than 1, and the maximum value near 50° is 1.21. The section near the vault first decreases and then increases as a whole. The upper chord at 55° has a minimum value of 0.63, while the lower chord changes gently at 10° to 75°, with a minimum value of 0.81.

To sum up, under the $X+Y$ combined seismic excitation of the arch rib chord, with the angle changing between 0° and 90°, the maximum axial force appears under different working conditions and changing angles. The change of the upper and lower chord axial force and the ratio of the axial force has obvious spatiality.

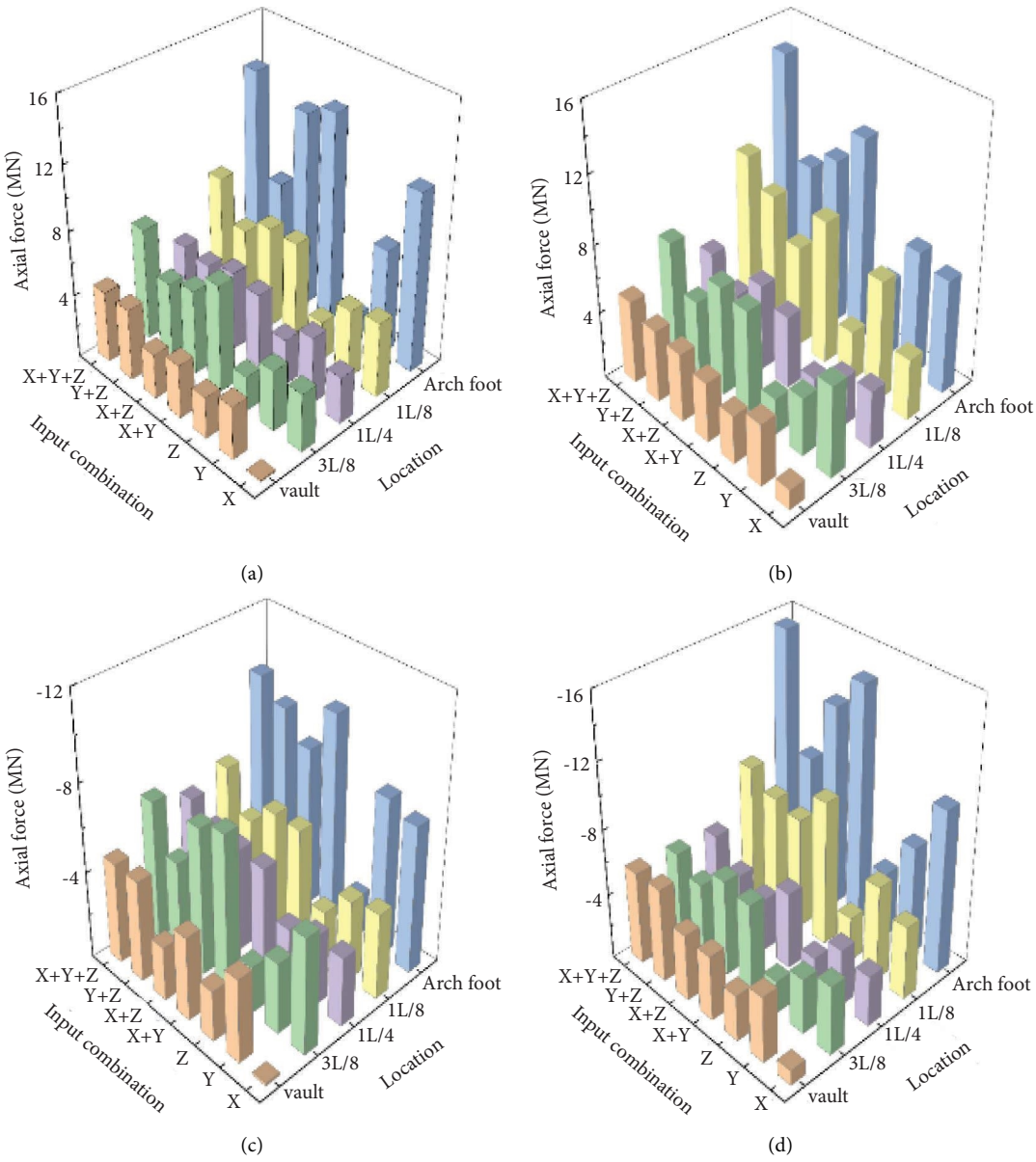

Figure 6: Axial force diagram of chord under multidimensional excitation. (a) Upper chord (*N*max), (b) lower chord (*N*max), (c) upper chord (*N*min), and (d) lower chord (*N*min).

6.2. Displacement Response. It can be seen from Figures 12–14 that the displacement changes along the *X* and *Z* directions of the arch-rib axis are mirror images, but they are reversed under the transformation from 0° to 90° along the arch-rib axis. The displacement change in the *Y* direction under the angle transformation is consistent; the displacement in the *X* direction increases first and then decreases, and the change along the arch rib has a high synchronization, which tends to be gentle in the range of 35°~60°. The maximum ratio is 1.19, and the minimum ratio is 0.96 at 90°. The displacement in the *Y* direction first decreases and then increases, and the change along the arch rib is consistent. The minimum ratio is 0.79 near 10°, and the change trend of each section appears at 55°. The difference is that the arch

Table 3: Chord axial force ratio table of two dimensions than one dimension.

Position	Direction	Upper chord				Lower chord			
		$X+Y$	$X+Z$	$Y+Z$	$X+Y+Z$	$X+Y$	$X+Z$	$Y+Z$	$X+Y+Z$
Arch foot	X	1.3	1.1	—	1.3	1.6	1.3	—	1.8
	Y	1.6	—	1.1	1.6	1.9	—	1.2	2.1
	Z	—	6.0	4.7	6.9	—	2.6	2.0	3.5
1L/8	X	1.4	1.4	—	1.6	2.1	1.6	—	2.2
	Y	1.5	—	1.2	1.7	1.3	—	1.2	1.4
	Z	—	2.5	2.0	2.9	—	2.2	2.7	3.1
1L/4	X	1.5	1.6	—	1.7	1.4	1.3	—	1.6
	Y	1.3	—	1.2	1.4	1.4	—	1.1	1.6
	Z	—	1.7	1.7	1.8	—	2.4	2.0	2.9
3L/8	X	1.6	1.3	—	1.5	1.2	1.3	—	1.3
	Y	2.0	—	1.3	1.9	1.7	—	1.3	1.8
	Z	—	2.8	2.1	3.1	—	3.0	2.2	3.0
Vault	X	3.8	2.8	—	4.9	3.6	3.8	—	5.0
	Y	1.0	—	1.3	1.3	1.0	—	1.3	1.4
	Z	—	1.1	1.9	1.9	—	1.4	1.8	1.9

Note. The values in the table are the ratios of the chord axial force amplitudes under two-dimensional and one-dimensional excitation.

Table 4: Chord axial force ratio table of three dimensions to two dimensions.

Position	Direction	Upper chord			Lower chord		
		$X+Y$	$X+Z$	$Y+Z$	$X+Y$	$X+Y$	$X+Z$
Arch foot	X	1.0	1.2	—	1.1	1.4	—
	Y	1.0	—	1.5	1.1	—	1.8
	Z	—	1.2	1.5	—	1.3	1.8
1L/8	X	1.1	1.1	—	1.0	1.4	—
	Y	1.1	—	1.4	1.1	—	1.2
	Z	—	1.2	1.5	—	1.4	1.1
1L/4	X	1.1	1.1	—	1.1	1.2	—
	Y	1.1	—	1.2	1.1	—	1.5
	Z	—	1.1	1.1	—	1.2	1.5
3L/8	X	0.9	1.2	—	1.1	1.0	—
	Y	1.0	—	1.5	1.1	—	1.4
	Z	—	1.1	1.5	—	1.0	1.4
Vault	X	1.3	1.8	—	1.4	1.3	—
	Y	1.3	—	1.0	1.4	—	1.1
	Z	—	1.7	1.0	—	1.4	1.1

Note. The values in the table are the ratios of the chord axial force amplitudes under three-dimensional and two-dimensional excitation.

foot to the vault increases in turn, and the maximum ratio is 1.59~2.01 at 90°. The Z direction displacement is relatively consistent from the arch foot to the 3 L/8 segment, showing a periodic increase/decrease in the arc segment. However, the change of vault displacement has a great asynchronicity, showing a trend of first decreasing and then increasing, and the minimum and maximum ratios are 0.74 and 1.24 at 35° and 90°, respectively.

To sum up, under the $X + Y$ combined seismic excitation of the arch rib chord with the angle changing from 0°~90°, the change trend of the displacement in the X and Y directions is relatively consistent, and the displacement change in the Z direction has obvious asynchronicity. The range of displacement ratio in the Z direction is 0.96~1.19, 0.79~2.01, and 0.74~1.24, respectively, and the maximum ratio in the Y direction of the vault section has nearly doubled.

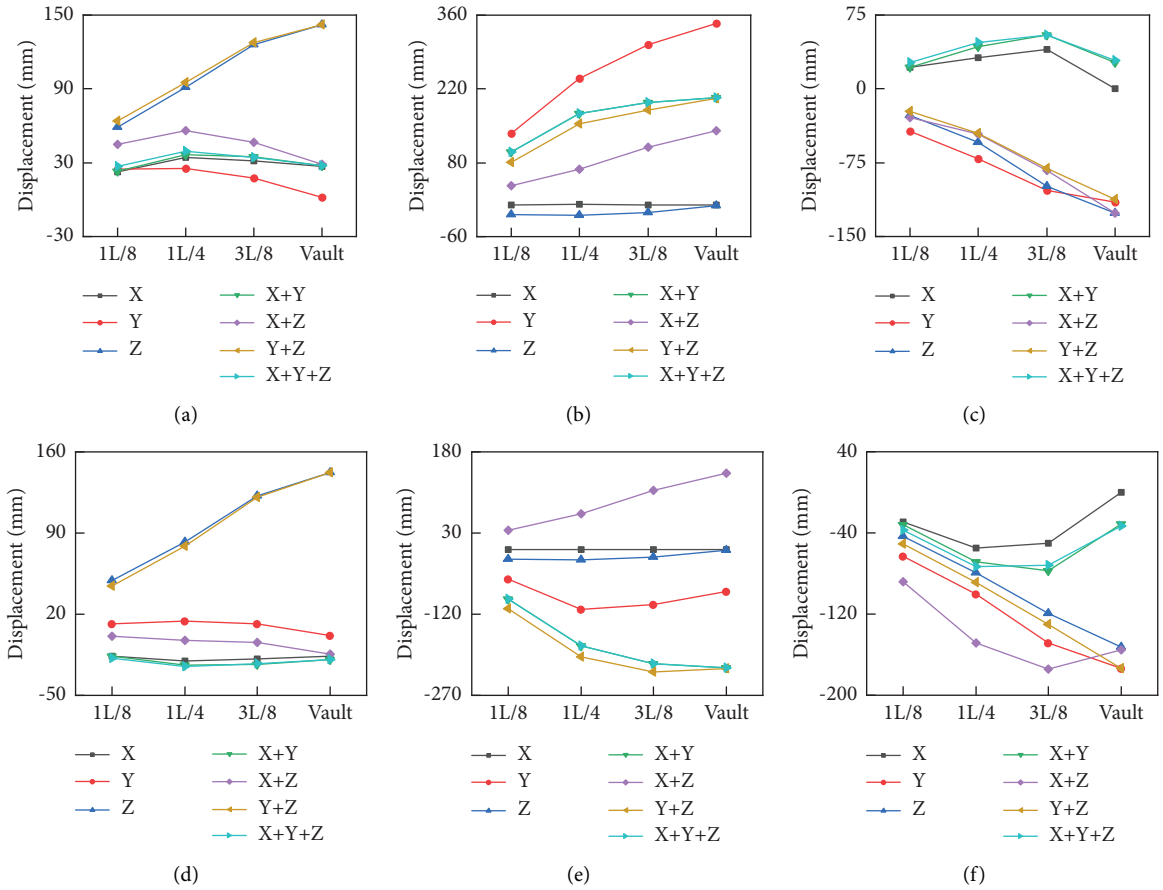

Figure 7: Upper chord displacement diagram under multidimensional excitation. (a) X direction (Nmax), (b) Y direction (Nmax), (c) Z direction (Nmax), (d) X direction (Nmin), (e) Y direction (Nmin), and (f) Z direction (Nmin).

Table 5: Upper chord displacement ratios.

Direction	Position	$X+Y$	$X+Z$	$Y+Z$	$X+Y+Z$
X	1L/8	1.0	1.1	—	1.2
	1L/4	1.1	1.1	—	1.2
	3L/8	1.1	1.0	—	1.1
	Vault	1.1	1.0	—	1.1
Y	1L/8	1.0	—	1.0	1.0
	1L/4	1.0	—	1.0	1.0
	3L/8	1.0	—	1.0	1.0
	Vault	1.0	—	1.0	1.0
Z	1L/8	—	3.7	1.7	4.0
	1L/4	—	4.0	1.7	4.7
	3L/8	—	4.5	2.4	6.3
	Vault	—	1.1	2.3	2.3

Note. The values in the table are the ratios of the chord displacement amplitudes under multidimensional and single-dimensional excitation.

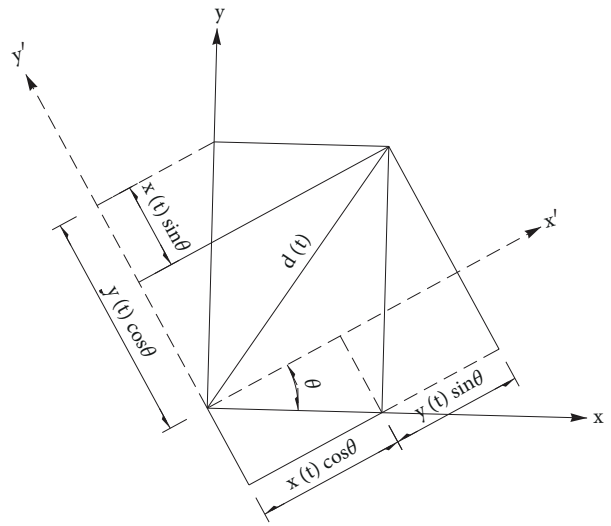

Figure 8: Coordinate transformation diagram.

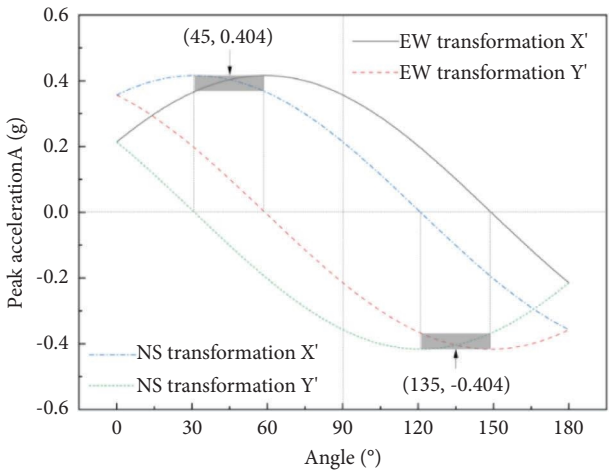

Figure 9: Coordinate transformation peak acceleration.

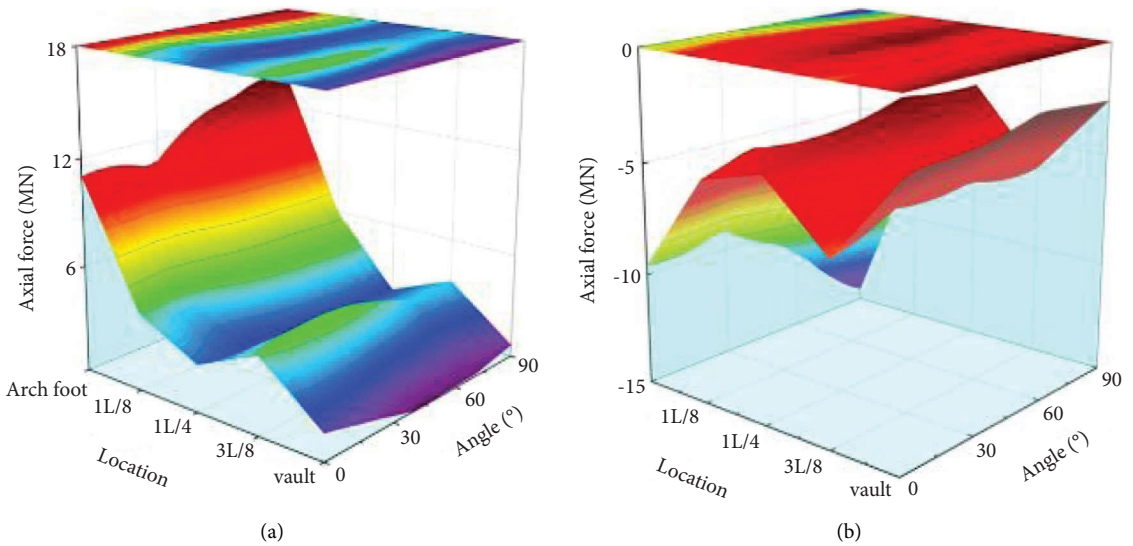

(a) (b)

Figure 10: Continued.

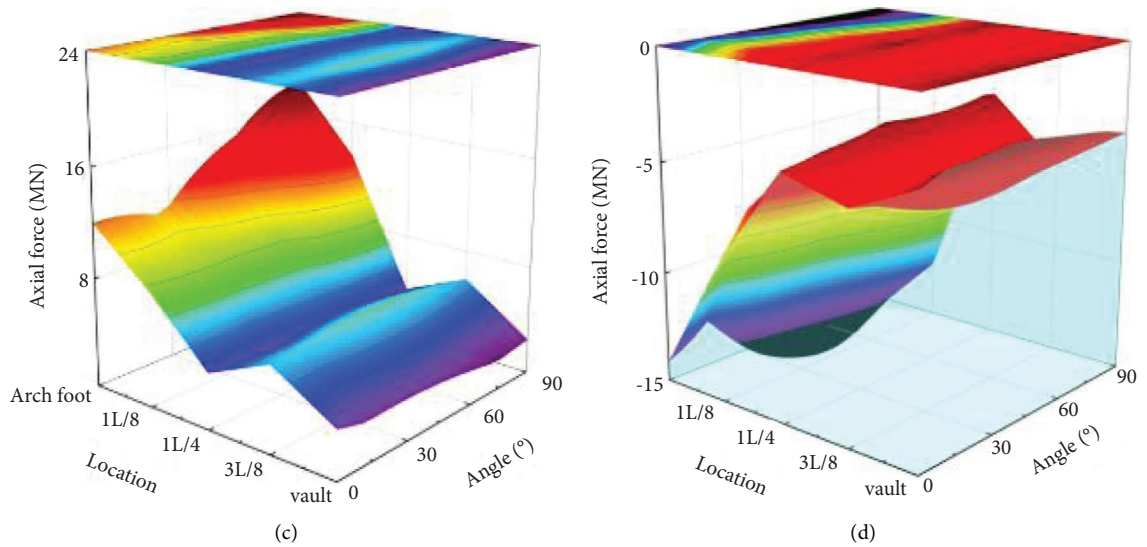

FIGURE 10: Chord axial force diagram under 0–90° transformation excitation. (a) Upper chord (*N*max). (b) Upper chord (*N*min). (c) Lower chord (*N*max). (d) Lower chord (*N*min).

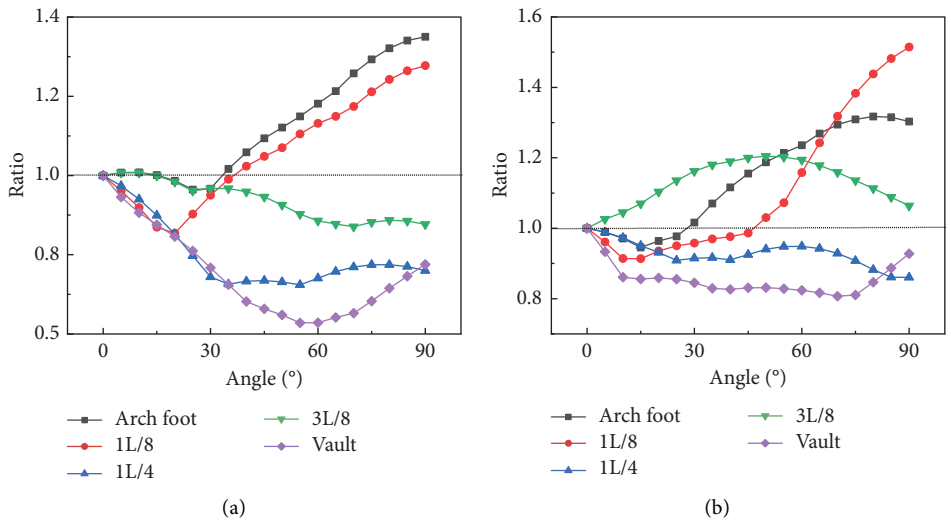

FIGURE 11: Upper chord axial force ratio table under 0–90° transformation excitation. (a) Upper chord axial force ratio diagram. (b) Lower chord axial force ratio diagram.

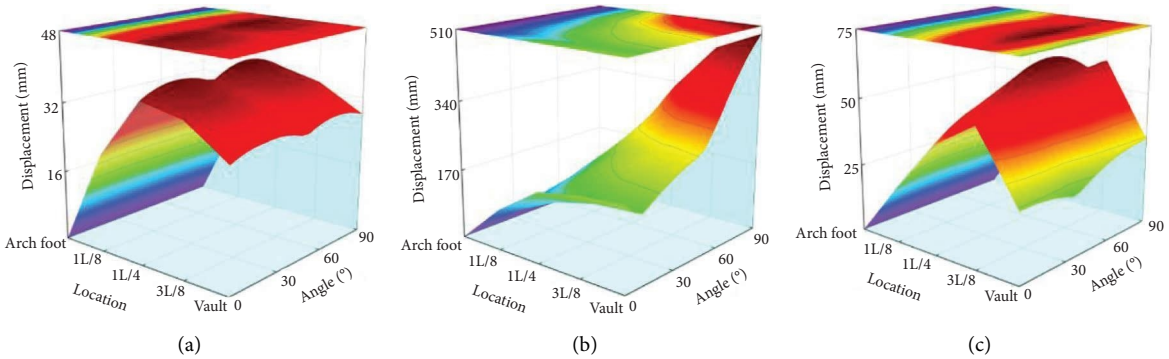

FIGURE 12: Upper chord displacement diagram for *N*max working condition under $X+Y$ combined excitation. (a) X direction, (b) Y direction, and (c) Z direction.

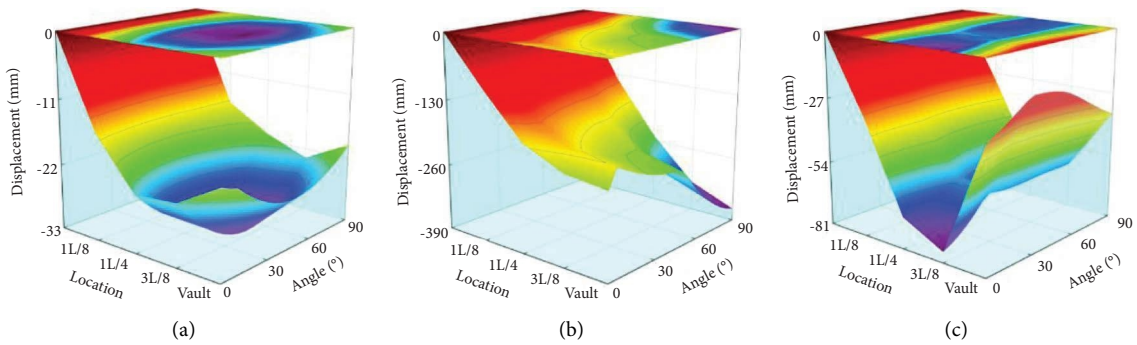

Figure 13: Upper chord displacement diagram for *N*min working condition under $X + Y$ combined multiangle excitation. (a) X direction, (b) Y direction, and (c) Z direction.

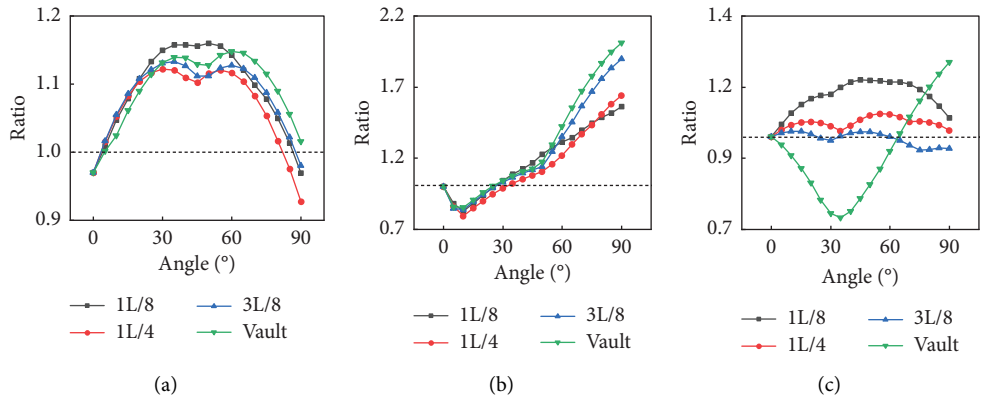

Figure 14: Upper chord displacement ratio under the $X + Y$ combined multiangle excitation. (a) X direction, (b) Y direction, and (c) Z direction. *Note*. The ratio in the figure is the ratio of the chord displacement variation amplitude of the $X + Y$ combination under multiangle and 0° seismic excitation.

7. Conclusions

(1) The composition of the long-span top-loaded arch bridge expands at the same time in the longitudinal and vertical dimensions, and the vibration form has obvious spatial coupling. The main mode shape of the arch rib is out-of-plane bending-torsional coupled vibration, the mode shape is relatively concentrated, and the mass of vibration mode participation has multidirectional and multiangle correlation.

(2) Under multidimensional combined excitation, with the increase of excitation dimension, the value and relative ratio of chord axial force are increasing. The maximum axial force ratio of $X + Y$ to X and Y is 2.1 and the maximum axial force ratio of $X + Y + Z$ to $X + Y$, $X + Z$, and $Y + Z$ is 1.4, 1.8, and 1.8. The axial force response has obvious three-dimensional superposition.

(3) The displacement of X and Y directions under combined excitation is independent, and the displacement of Z direction is its coupling term, but the displacement under $X + Y + Z$ combined excitation is only 10% larger than that under $X + Z$ and $Y + Z$ combined excitation.

(4) Under the combined excitation of $X + Y$, with the angle changing from 0° to 90°, the changes of the upper and lower chord axial force and the ratio of the axial force at different positions along the longitudinal direction of the arch rib and the same section have obvious spatial characteristics, the variation range of the upper chord axial force is 0.63~1.35, and the variation range of the axial force of the lower chord is 0.81~1.51.

(5) Under the combined excitation of $X + Y$, with the angle changing from 0° to 90°, the change trends of the displacements in the X and Y directions are relatively consistent, and the displacement changes in the Z direction have obvious asynchronicity. The change ranges of the displacement ratios in the X, Y, and Z directions are 0.96~1.19, 0.79~2.01, and 0.74~1.24, respectively, and that in the Y direction of the vault section has increased by nearly onefold.

The mass and stiffness distribution of long-span deck CFST arch bridge is spatial; the vibration in all directions is coupled. Under multidimensional combined excitation and multiangle combined excitation, the axial force and displacement response of chords have increased to varying degrees. Therefore, for the seismic response of this bridge

type, $X+Y+Z$ multidimensional combined excitation and $X+Y$ transformation angle combined excitation should be solved.

Data Availability

The data that support the findings of this study can be obtained from the corresponding author upon reasonable request.

Conflicts of Interest

The authors declare that they have no conflicts of interest.

References

[1] J. L. Zheng and J. J. Wang, "Concrete-filled steel tube Arch bridges in China," *Engineering*, vol. 4, no. 1, pp. 143–155, 2018.

[2] Z. Li, L. Ren, and H. Yuan, "Performance-based rapid evaluation method for post-earthquake traffic capacity of bridge system," *IOP Conference Series: Earth and Environmental Science*, vol. 791, no. 1, p. 012070, 2021.

[3] X. S. Xia, S. Y. Dai, and Z. W. Liu, "Seismic conceptual design method of long-span arch bridges," *Earthquake Engineering and Engineering Dynamics*, vol. 37, no. 2, pp. 90–96, 2017.

[4] L. L. Xie and C. H. Zhai, "Study on the severestreal ground motion for seismic design and analysis," *Acta Seismologica Sinica (Chinese edition)*, vol. 16, no. 3, pp. 260–271, 2003.

[5] D. Y. Zhang, H. Y. Jia, S. X. Zheng, W. C. Xie, and M. D. Pandey, "A highly efficient and accurate stochastic seismic analysis approach for structures under tridirectional nonstationary multiple excitations," *Computers & Structures*, vol. 145, pp. 23–35, 2014.

[6] W. W. Luo, H. F. Li, and B. A. Cao, "Seismic performance of eccentrically-compressed steel pier under multi-directional earthquake loads," *Earthquake Engineering and Engineering Dynamics: English Edition*, vol. 20, no. 3, pp. 171–189, 2021.

[7] F. Fan, H. L. Qian, and L. L. Xie, "Applications of the severest ground motion to anti-seismic design for reticulated shells," *World Earthquake Engineering*, vol. 19, no. 3, pp. 17–21, 2003.

[8] M. Sibo and D. Yang, "Stochastic response of a coastal cable-stayed bridge subjected to multi-dimensional and multi-supported earthquake and waves," *Journal of earthquake and tsunami*, vol. 15, no. 2, Article ID 2150006, 2021.

[9] S. D. Xue, X. S. Wang, and Z. Cao, "The college of architecture and civil engineering," *World Earthquake Engineering*, vol. 18, no. 1, pp. 34–40, 2002.

[10] Y. L. Zhang, Y. Wang, X. C. Chen, L. S. Yu, and C. C. Liu, "Spatial seismic response of long-spandeck rail way steel truss arch bridge under multi-dimensional excitation," *China Railway Science*, vol. 41, no. 5, pp. 56–63, 2020.

[11] S. Farahmand-Tabar and M. Barghian, "Seismic assessment of a cable-stayed arch bridge under three-component orthotropic earthquake excitation," *Advances in Structural Engineering*, vol. 24, no. 2, pp. 227–242, 2020.

[12] F. Y. Huang, C. Fu, Y. Z. Zhuang, and Z. H. Xiong, "Experiment on seismic performance of concrete filled steel tubular arch- rib under multi-shaking-tables," *Thin-Walled Structures*, vol. 116, pp. 212–224, 2017.

[13] H. Z. Luo, D. S. Zhu, and J. Y. Yu, "Seismic response characteristics of a rib-arch bridge," *Journal of Chong qing Jiao tong University:Natural Science*, vol. 38, no. 6, pp. 30–36, 2019.

[14] D. H. Chen and W. H. Guo, "Spatial seismic response analysis of long-span steel truss arch bridge," *Journal of Central South University:Natural Science*, vol. 41, no. 4, pp. 1290–1596, 2010.

[15] Y. W. Dai, C. Liu, W. F. Li, and L. Tian, "Research on tuned mass damper for vibration control of tower under multi-dimensional seismic excitations," *Applied Mechanics and Materials*, vol. 353-356, pp. 2181–2186, 2013.

[16] C. H. Zhao and Z. X. Zhou, "Stochastic response of a long-span x-type concrete filled-insteel tube arch bridge to multi-camponent seismic excitation," *Earthquake Engineering and Engineering Vibration*, vol. 25, no. 3, pp. 87–92, 2005.

[17] D. Y. Zhang, X. Li, W. M. Yan, W. C. Xie, and M. D. Pandey, "Stochastic seismic analysis of a concrete-filled steel tubular (CFST) arch bridge under tridirectional multiple excitations," *Engineering Structures*, vol. 52, pp. 355–371, 2013.

[18] X. Z. Li, D. H. Yang, K. N. Lei, L. Xiao, and S. Y. Dai, "Seismic response of continuous beam-arch bridge under spatially varying ground motions," *Journal of Southwest Jiaotong University*, vol. 56, no. 2, pp. 221–228, 2021.

[19] X. Z. Li, Q. Y. Hong, H. J. Lei, and Z. J. Liu, "Effect of input directions of seismic ground motionon seismi cresponses of a rail way extradosed bridge," *Bridge Construction*, vol. 45, no. 1, pp. 26–32, 2015.

[20] T. Wang, E. D. Guo, and L. N. Zhang, "The critical direction of earthquake input for dynami canalysis of a long span cable-stayed bridge," *World Earthquake Engineering*, vol. 23, no. 4, pp. 107–111, 2007.

[21] C. Y. Liu, G. X. Yu, X. S. Fan, C. Q. Guo, and F. Li, "Seismic behavior and finite element analysis of reinforced concrete short columns impacted by oblique earthquakes," *Advances in Civil Engineering*, vol. 2020, pp. 1–15, Article ID 9260203, 2020.

[22] M. H. Sun, B. T. Sun, G. L. Hou, and F. Fan, "Study on the main direction of ground motion and its effect on the dynamic response of structure," *China Civil Engineering Journal*, vol. 53, no. 2, pp. 150–155, 2020.

[23] J. W. Zhang, M. C. Li, S. Han, and G. H. Deng, "Estimation of seismic wave incident angle using vibration response data and stacking ensemble algorithm," *Computers and Geotechnics*, vol. 137, no. 5, p. 104255, 2021.

[24] H. J. Shen, H. Wang, W. Z. Zheng, R. J. Liang, B. Sha, and J. H. Xu, "Vulnerability analysis of round-end piers of high-speed railway bridges under multi-dimensional seismic action," *Earthquake Research*, vol. 44, no. 2, pp. 225–231, 2021.

[25] B. F. Dou, X. Yang, and C. Dou, "Dynamic characteristic and seismic response of arch structures," *Structural Engineers*, vol. 38, no. 4, pp. 82–89, 2022.

[26] L. L. Wan, R. C. Ji, and X. S. Xia, "Research on seismic isolation design of large span extradosed cable stayed bridge on high speed railway," *Railway Engineering*, vol. 61, no. 12, pp. 31–35, 2021.